Digital Alloy Contact Layers for Perovskite Solar Cells

Olivia Sergiovanni[b], Ekraj Dahal[a], Bin Du[b], Benjamin Isenhart[b], Sean Dunfield[c,d], Joseph J. Berry[d], Matthew S. White[b,a,*]

[a]*Materials Science Program, University of Vermont, 82 University Pl., Burlington, Vermont 05405, United States*
[b]*Department of Physics, University of Vermont, 82 University Pl., Burlington, VT 05405, United States*
[c]*Materials Science & Engineering Program, University of Colorado, Boulder, Colorado 80303, United States*
[d]*National Renewable Energy Laboratory, Golden, Colorado 80401, United States*

Abstract

Thin film optoelectronic devices commonly require an individual material to perform multiple functions, but the physical properties of single-composition materials often cannot be tuned to optimize these diverse requirements. The electron selective contact layer in perovskite solar cells is a prime example. The material must simultaneously have optimal conduction band alignment, facilitate carrier extraction, prevent recombination, and provide a chemically stable interface with the notoriously volatile perovskite semiconductor. The pulse-by-pulse nature of the thin-film deposition method pulsed laser deposition (PLD) provides an opportunity to form material alloys where the chemical composition is controlled at the nanometer scale. These digital alloys may prove to be a powerful materials class to meet some of the multifunctional needs of thin film devices. Using PLD to make electron transport layers from ZnO and MgZnO targets, we demonstrate that digital alloy gradients can be tuned to significantly outperform either of the parent materials in perovskite solar cells.

Keywords: Perovskite, digital alloy, solar cell, electron transport layer

1. Introduction

Metal oxides, due to their robust nature and tunable properties, have been used to perform every function in photovoltaic devices.[1] These functions often require specific thermal, optical, chemical, surface, and electrical properties which are often anti-correlated. They are used as a transparent conductive electrode, [2, 3, 4] a rectifying carrier-specific contact layer, [5, 6, 7, 8, 9, 10, 11, 12] a structural/morphological scaffold, [13, 14] or an n-type acceptor in heterojunction solar cells. [14, 15] In addition to their use as the absorber[1, 16], oxides have been employed extensively as electron transport layers (ETL) (TiO_2, SnO_2, ZnO)[17, 18, 19] and hole transport layers (HTL) (NiO, WO_3) [20, 21] in perovskite solar cells. Functioning as the ETL in a perovskite solar cell, the oxide layer is required to promote the collection of electrons from the bulk perovksite, inhibit electron-hole recombination, and form a chemically stable interface that prevents phase separation and photocatalytic decomposition of the perovskite. [17, 18, 19] An intrinsic (TiO_2) ETL has been shown to occupy the region of the strongest electric field, indicating that the oxide-perovskite interface is the location of the primary p-n heterojunction that drives charge separation in a perovskite solar cell.[22] Efficient extraction of carriers from the cell mandates precise band alignment at the heterojunction interface, high carrier mobility in the bulk, strong band-bending near the interface (high bulk carrier concentration), and low interfacial carrier concentration. [9, 23] It is evident that the multiple requirements placed on this one layer dictate different material properties at different positions within the film, specifically bulk and interfacial properties. Given that the layer thickness ranges from 10 nm to 200 nm, the requirements demand positional control of the material composition at the nano-scale.

Pulsed laser deposition (PLD) allows layer-by-layer compositional control during ETL deposition [24, 25, 26, 27] by changing the material target between sequential pulses creating a *digital alloy* thin film. Digital alloys are generally described as short-period superlattice films that takes on desired bulk properties.[28, 29, 30, 31, 32] The digital alloy films in this work employ discrete steps at both the nanometer and the sub-monolayer scale to achieve the desired properties. The films are deposited in bursts as individual laser pulses ablate the surface of the material target, requiring roughly 10-50 pulses to form each monolayer of the film. Target-switching has previously been used to create alloys, [33, 34] and digital-alloy superlattices of complex oxides for advanced ferroelectrics, quantum paraelectrics, ferromagnetics, Mott-Hubbard insulators, and high-temperature superconductors. [26, 35, 36, 37, 38, 39, 40, 41, 42, 43] Ohtomo et al. have demonstrated remarkable optical properties of band-gap modulated superlattices of ZnO and $Mg_xZn_{1-x}O$ produced by PLD and molecular beam epitaxy. [44, 45, 46, 47, 48] PLD yields an unparalleled degree of structure and property control among the possible processing methods. According to Christen and Eres, it is "the tool of choice for the growth of complex oxide materials." [24]

In this work, we have used PLD to produce digital alloy ZnO-based ETLs for perovskite solar cells. The solar cells employ a formamidinium/methylammonium/Cs triple cation, I/Br dual

*Corresponding Author
Email address: mwhite25@uvm.edu (Matthew S. White)

anion perovskite (FAMACs) active layer with Spiro-OMeTAD HTL. While ZnO is not a state-of-the-art ETL material in terms of either device performance or stability, it does offer several key properties that allow us to explore the potential of digital-alloy films. The *n*-type carrier concentration in ZnO may be controlled by doping [3, 45, 49, 50, 51, 52, 53, 54], or by controlling the oxygen partial pressure during deposition. [9]. The conduction band edge may be raised and band-gap widened up to 800 meV by isovalent-substitution of Mg up to 40%. [23] We use the combination of oxygen partial pressure and a per-shot selection of ZnO and $Zn_{0.83}Mg_{0.17}O$ targets to create digital alloys with controlled conductivity and conduction band energy at each step of the layer-by-layer growth. These alloys can be tuned to meet the complex bulk and surface requirements of transport layer films, allowing the realization of devices with improved photovoltaic performance compared to either of the parent materials.

2. Experimental Details

2.1. Materials

The ZnO and $Mg_{0.17}Zn_{0.83}O$ targets for PLD were obtained from Plasmaterials, indium-tin oxide (ITO) patterned glass substrate was purchased from Thin Film Devices, SnO_2 (15% in H_2O colloidal dispersion) from Alfa Aesar. For the FAMACs perovskite, FAI and MABr were purchased from Dyesol, PbI_2 and $PbBr_2$ from Alfa Aesar, Spiro-OMeTAD from Sigma Aldrich, molybdenum(VI) oxide (99.99%) from Sigma Aldrich, and silver (99.99%) from Kurt J. Lesker. All the chemical reagents were used without any further purification.

2.2. PLD Digital Alloys

PLD was used to fabricate thin films of ZnO with varied Mg substitution concentration up to 17% at a range of oxygen partial pressures from 5 mTorr to 50 mTorr. The deposition rate was calibrated for ZnO as 10 pulses per Å, for $Mg_{0.17}Zn_{0.83}O$ as 20 pulses per Å. The energy per pulse of the laser was roughly 750 mJ. Switching between targets with varying pulse ratio allows for deposition of films with Mg concentration ranging from 0 to 17%.

2.3. Device Fabrication

The FAMACs active layer was deposited from a solution prepared from a mixed FAMACs powder dispersed by ball milling.[55] A salt mixture of 3.54 g FAI, 0.461 g MABr, 10.44 g PbI_2, 1.511 g $PbBr_2$, and 0.339 g CsI was ball milled over night to ensure complete mixing. 760 mg of the mixture was dissolved in 1 ml of a DMSO:DMF solvent mixture at a 4:1 volume ratio. The HTL solution was prepared by adding 72 mg Spiro-OMeTAD and 28 μl of 4-tert-butylpyridine to 1 mL chlorobenzene. 17 μl of dopant stock solution was added, which consisted of 520 mg/mL bis(trifluoromethanesulfonyl)imide (Li-TFSI) in acetonitrile. For control devices, the ETL solution was prepared by diluting SnO_2 (15% in H_2O colloidal dispersion) with deionized water at a 1:4 volume ratio.

Perovskite solar cells were fabricated on ITO patterned glass substrates. All glass and ITO substrates were cleaned by sequential ultrasonic brush in water with Liquinox detergent, rinsed with deionized water, ultrasonic bath with acetone, and isopropanol for 15 minutes each followed by a 15 min UV-ozone cleaning. For control devices, the SnO_2 nanoparticle solution spin-coated at 3000 rpm for 30 seconds and annealed for 30 minutes at 150 °C was used as the ETL. Digital alloy ETLs were deposited with 25 nm total thickness on ITO as described above. All ETLs were treated with a 15 min UV-ozone cleaning. The slides were moved to a nitrogren environment and the solution-processed FAMACs perovskite layer was applied by spin coating at 1000 rpm for 10 seconds then 6000 rpm for 20 seconds. An anti-solvent chlorobenzene rinse was applied via dynamic spin 14 seconds into the 6000 rpm cycle. The slides underwent a post annealing treatment for 60 minutes at 105 °C then were removed from the hot plate and allowed to cool for 1 minute before spin coating the Spiro-OMeTAD HTL at 5000 rpm for 30 seconds. Following deposition of the HTL, slides were moved to a dry environment in air for 12+ hours to allow the SpirO-OMeTAD to oxidize. Cathodes were deposited in a glovebox-integrated thermal evaporator (Angstrom Engineering, Inc.). MoO_x of thickness 10 nm is deposited at a rate of 0.1 $Å s^{-1}$ as a hole collecting interlayer and aluminum top metal electrode of 100 nm thickness was deposited at a rate of 0.5 $Å s^{-1}$ with a base pressure of 1.0×10^{-7} Torr. Completed devices were stored in a nitrogen glove box (<1 ppm H_2O and O_2) before testing.

2.4. Characterization

Sheet resistance was characterized using Four Point Probe. Thickness was measured using a profilometer (Dektak 8). Electrical transport characterizations were carried out using Hall effect measurements on ZnO and $Mg_{0.17}Zn_{0.83}O$ in the van der Pauw geometry using the Physical Property Measurement System (PPMS) (Quantum Design PPMS Dynacool) by applying an external magnetic field from -10 T to 10 T.

The crystallinity and preferred crystal orientation of ZnO (deposited at 5 mTorr, 10 mTorr, 20 mTorr, 30 mTorr, 40 mTorr, 50 mTorr), and the FAMACs perovskite on ZnO, $Mg_{0.17}Zn_{0.83}O$ and SnO_2 annealed at 110°C were characterized using X-ray diffractometer D8 Discover, Bruker with a Hi-Star 2D area detector using Cu Kα radiation (1.54 Å).

The solar cell device performance measurement was taken under a simulated AM 1.5G illumination 100 mW cm^{-2}, Oriel Sol3A Class AAA Solar Simulator by Newport at room temperature under nitrogen atmosphere. The solar simulator was calibrated with an encapsulated Si reference diode with KG 2 filter. Devices were masked with a metal aperture with size 0.059 cm^2 and swept between -0.5 V and 1.5 V with a step size of 0.01 V at a rate of 0.8 V/s in both forward and reverse directions. Reverse-scans are reported here.

Table 1: Electrical properties of ZnO PLD thin films at room temperature, deposited at various O_2 partial pressures.

O_2 partial pressure [mTorr]	Resistivity [Ω cm]	Electron mobility [cm^2/Vs]	Carrier concentration [cm^{-3}]
5	2.19×10^{-3}	15.96	1.79×10^{20}
30	8.26×10^{-2}	1.34	5.64×10^{19}
40	1.06×10^{-1}	1.12	5.30×10^{19}
50	2.04×10^{-1}	0.64	4.76×10^{19}

3. Results and Discussion

3.1. Digital Alloy Oxide Films

We first characterize the range of physical properties attainable using the digital alloy PLD method in our ZnO-based ETL layers. By varying the O_2 partial pressure during deposition from a ZnO target, we were able to control the carrier concentration and overall conductivity of the oxide film. ZnO films were deposited onto glass slides at O_2 partial pressures ranging from 5 mTorr to 50 mTorr. Electrical transport properties of the films were measured using a 4-point probe and a Hall measurement system using a van der Pauw configuration under a 10 T magnetic field. Resistivity (ρ), electron mobility (μ), and bulk carrier concentration (n), were measured and are shown for several partial pressures in Table 1.

The resistivity of the ZnO films ranged from 2.04×10^{-1} Ω cm at 50 mTorr partial pressure to 2.19×10^{-3} Ω cm at 5 mTorr. Lower O_2 partial pressure during deposition corresponds to a higher conductivity due to a combination of roughly 4-fold increase in carrier concentration and roughly 25-times higher electron mobility.

Deposition of thin films from a target consisting of $Mg_{0.17}Zn_{0.83}O$, at 50 mTorr O_2 partial pressure results in highly insulating films. The per-pulse deposition rate was 20 pulses per Å for this $Mg_{0.17}Zn_{0.83}O$ target, and 10 pulses per Å for the pure ZnO target. Switching between these targets with well defined pulse-per-target ratio (ZnO:MgZnO) allowed us to generate films with 5.67% (1:1), 8.5% (1:2), and 11.33% (1:4) Mg, blending the two target compositions at the monolayer level. According to Ohtomo[45] and Olson[23], this range increases the bandgap of the ZnO by 400 meV, from roughly 3.2 - 3.3 eV to roughly 3.6 - 3.7 eV as a linear function of Mg concentration. The bandgap increase is primarily due to a raising of the conduction band level.[45, 23, 56, 57, 49] All of the ZnO films with varying Mg content and deposited at different O_2 partial pressures were found to be ZnO wurtzite structure, as has been previously reported for similar PLD films.[57] The wide bandgap materials and the very thin (5 to 25 nm) films show no significant increase in absorption or reflection of visible light which could potentially interfere with photocurrent generation in solar cells, as can be seen in Figure S1.

3.2. Perovskite Oxide Interfaces

Fixed-composition oxide thin films are routinely used as ETLs in perovskite solar cells. Here we compare the photovoltaic performance of devices employing thin films of ZnO and $Mg_{0.17}Zn_{0.83}O$ deposited by PLD to a film of SnO_2 deposited by spin coating from a nanoparticle suspension, a state-of-the-art ETL in terms of device performance and stability.[58] The J-V curves for these devices are shown in Fig. 1. The SnO_2 device showed significantly higher performance than the other contact layers with a power conversion efficiency (PCE) of 17.2%. The ZnO and $Mg_{0.17}Zn_{0.83}O$ devices showed power conversion efficiency (PCE or η) values of 2.5% and 1.1% respectively. Both of the devices employing the PLD oxide ETL films show a nearly four-fold reduction in short circuit current density (J_{SC}), a 100 mV lower open circuit voltage (V_{OC}), and significantly lower fill factor (FF) compared to the SnO_2-based device. The $Mg_{0.17}Zn_{0.83}O$-based device shows clear field-dependent carrier extraction and a counter-diode region from roughly 0.7 to 1.2 V forward bias where neither injection nor extraction of photogenerated carriers occurs efficiently. This is very likely due to the low conductivity and highly insulating nature of the 25 nm thick $Mg_{0.17}Zn_{0.83}O$ layer. The poor performance of the ZnO-based device requires more explanation, as ZnO has been shown to act as a high-performance ETL for various PV technologies.[5, 59, 60, 61]

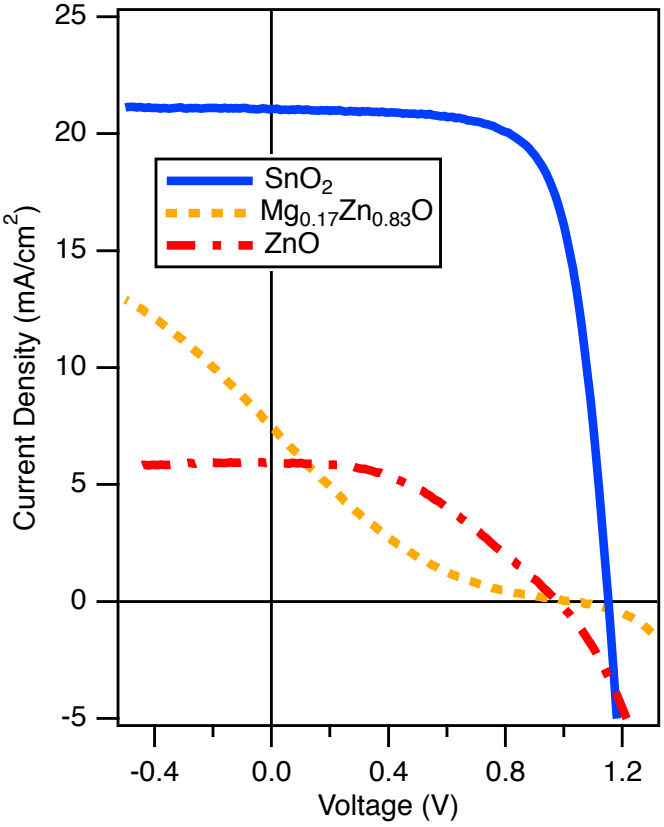

Figure 1: Performance of perovskite solar cells with SnO_2, ZnO (50 mTorr), and $Mg_{0.17}Zn_{0.83}O$ (50 mTorr) ETLs.

The surface chemistry of ZnO presents a significant problem for use in perovskite solar cells. ZnO has been shown to protonate methylamonium and produce PbI_2 at a perovskite interface upon thermal annealing.[62] The XRD patterns of FAMACs perovskite films deposited onto the oxide films employed as ETLs in the devices above are shown in Fig. 2. A PbI_2 (001)

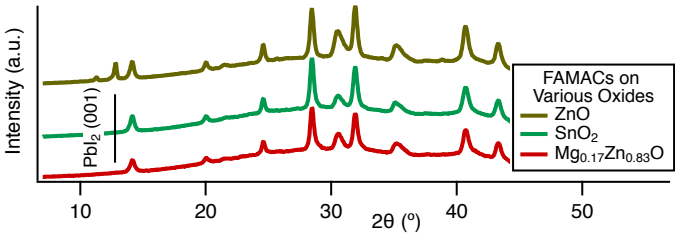

Figure 2: XRD patterns of the FAMACs Perovskite layer on the surface of ZnO (PLD), SnO_2 (from solution), and $Mg_{0.17}Zn_{0.83}O$ (PLD). All films were annealed at 110°C for 30 min.

peak is clearly evident at the ZnO/FAMACs interface, that is not present with the other oxide films. The FAMACs perovskite undergoes a decomposition into PbI_2 at the ZnO interface, which results in the low performance of the solar cells employing a ZnO ETL.[63] While $Mg_{0.17}Zn_{0.83}O$ may provide a more chemically stable interface than ZnO, it is limited as an ETL by its charge transport properties. The demand for an ETL material to serve different functions at the interfaces and in the bulk motivates the development of digital alloy contact layers with controlled composition at each layer of the film.

3.3. Digital Alloy Gradient ETLs in Perovskite PV

An efficient ETL must achieve precise conduction band alignment while maintaining a stable interface and efficient charge extraction. On their own neither ZnO nor $Mg_xZn_{(1-x)}O$ can meet all of these requirements. By combining the two materials using the digital alloy technique, the favorable properties of each material may be simultaneously optimized for device performance. To test this hypothesis, we designed three different Digital Alloy contact layers, based on the single-composition ETLs which indicated that interface between ZnO and the FAMACs perovskite is chemically unstable, while $Mg_{0.17}Zn_{0.83}O$ provides a stable interface but the bulk resistivity inhibits carrier extraction from the device. A schematic showing these three ETLs in the perovskite solar cell device architecture is shown in Fig. 3.

Our first digital alloy ETL film directly addresses these challenges by applying a 5 nm $Mg_{0.17}Zn_{0.83}O$ interface capping layer to 20 nm of bulk ZnO deposited at an O_2 partial pressure of 5 mTorr to minimize resistivity. This interface capping layer does not result in an improvement in solar cell performance. The brown dashed J-V curve in Fig. 4 shows residual counter-diode behavior from the capping layer, and an overall poor carrier extraction resulting in low J_{SC}. Yet PLD digital alloys allow a significantly higher degree of control over the material composition.

Our second digital alloy ETL utilizes a gradient of Mg concentration to gradually raise the band gap energy through the film. The partial pressure during deposition was held constant at 5 mTorr while the Mg dopant concentration was increased from 0% to 17% in 5 steps. This is designed to preserve a higher conductivity film, while creating an energetic staircase in the ETL conduction band to drive photo-generated electrons away from perovskite/oxide interface. Perovskite solar cells based on this Bandgap Gradient digital alloy ETL (Fig. 4) show higher power conversion efficiency than either of the devices based on the ZnO or the $Mg_{0.17}Zn_{0.83}O$ ETL shown in Fig. 1. However, the high conductivity appears to increase carrier recombination at the interface, resulting in a low V_{OC} and FF.

Table 2: Single-composition (first three) and digital alloy (last three) ETL based solar cell performance metrics.

ETL	V_{OC} [V]	J_{SC} [mA/cm^2]	FF	η [%]
SnO_2 (nanoparticle)	1.15	21.07	0.71	17.20
$Mg_{0.17}Zn_{0.83}O$	1.04	7.46	0.15	1.16
ZnO	0.98	5.92	0.42	2.44
Interface Capping	1.04	1.52	0.53	0.83
Bandgap Gradient	0.94	9.79	0.29	2.66
Bandgap & Conductivity Gradient	1.11	12.91	0.34	4.83

The third digital alloy ETL addresses this recombination using the same gradient in Mg concentration while also increasing the O_2 partial pressure from 10 mTorr to 50 mTorr over the 5 steps. The design of this Bandgap & Conductivity Gradient allowed for the bandgap energy to incrementally increase towards the perovskite interface while simultaneously decreasing the conductivity through the film, with the interfacial layer having the lowest carrier concentration. Device performance metrics for the three digital alloy ETLs can be seen in Table 2, and the J-V curves are shown in Fig. 4. It is clear that the digital alloy ETL where both the band alignment and the conductivity change in a five-step gradient from the ITO to the FAMACs interface results in the highest V_{OC}, J_{SC}, and power conversion efficiency of the digital alloy films, with performance significantly higher than either of the single-composition ZnO or $Mg_{0.17}Zn_{0.83}O$ ETLs. This represents a combination of improved chemical stability at the interface which prevents decomposition of the perovskite, and a balancing of the band-bending and energetic offset to encourage charge carrier separation and prevent recombination at the ETL/perovskite interface, which acts as the primary junction driving charge separation.[9, 22] The five-step gradient of conduction-band level and carrier concentration provides a series of energetic barriers for recombination, with increasing electric field strength at the critical interface with the perovskite. While the optimized digital alloy ZnO-based device does not compare favorably to the state-of-the-art SnO_2 ETL, partially due to the unoptimized active layer formulation and processing for this contact layer[64, 65, 66], it demonstrates that the degree of control afforded by digital alloy PLD films can be used to optimize materials for purposes where a constant composition would be insufficient.

4. Conclusions

We show that deposition of digital alloys can be used to combine favorable properties of two materials that, on their own, fail to meet the multifunctional demands placed on thin

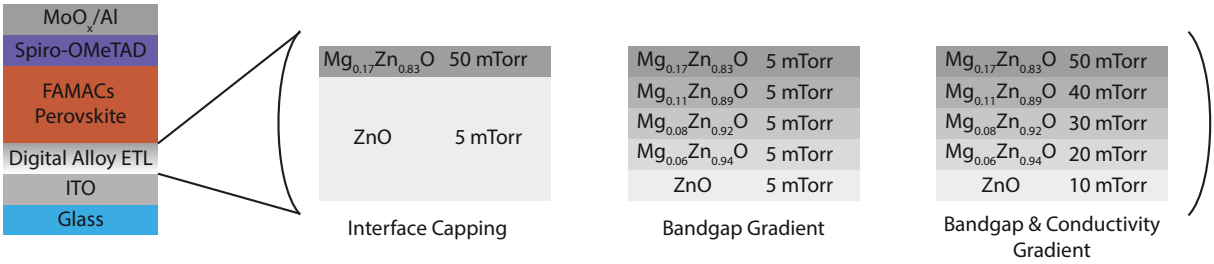

Figure 3: Device schematic of the perovskite solar cells with digital alloy ETLs, and a detailed schematic of the three digital alloy ETLs employed in this work. Total ETL thickness is 25 nm in each case.

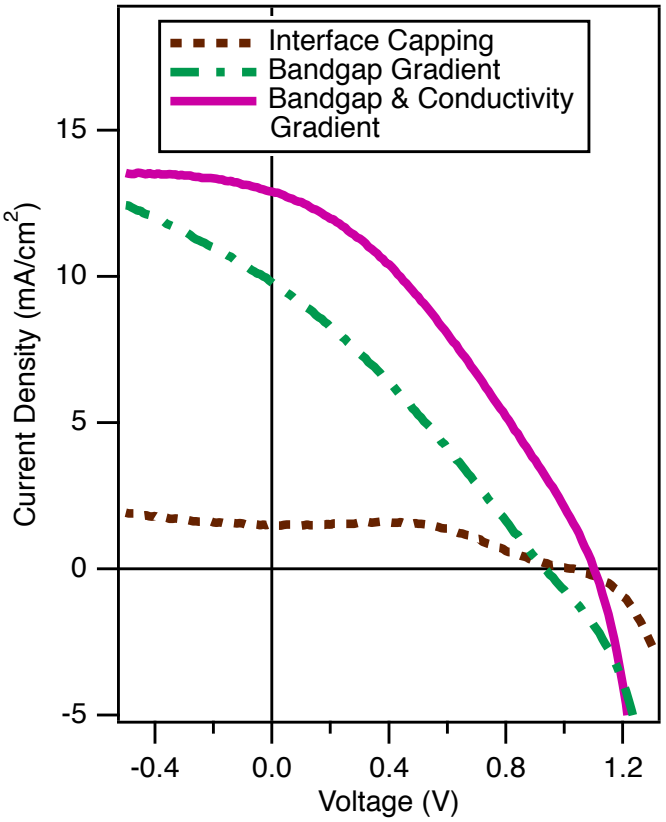

Figure 4: Performance of perovskite solar cell with various ZnO-based digital alloy ETLs.

films in optoelectronic devices. PLD films of both ZnO and $Mg_{0.17}Zn_{0.83}O$ are shown to perform poorly as ETLs in FAMACs perovskite solar cells. One creates a chemically unstable interface resulting in decomposition of the perovskite, and the other creates a low-conductivity region that prevents carrier extraction at low-field. Although ZnO presents an unsuitable interface, and $Mg_{0.17}Zn_{0.83}O$ presents bulk transport limitations, simply capping the ZnO bulk with an interfacial $Mg_{0.17}Zn_{0.83}O$ does not result in efficient collection and extraction of carriers. We show that PLD may be used to create digital alloy ETLs with finely controlled energetic and conductivity gradients, ultimately resulting in an ETL that significantly outperforms either of the parent materials.

CRediT authorship contribution statement

Olivia Sergiovanni: Investigation, Writing - Original Draft, Visualization. **Ekraj Dahal**: Investigation, Writing - review & editing. **Bin Du**: Investigation, Visualization. **Benjamin Isenhart**: Investigation, Visualiztion. **Sean Dunfield**: Investigation. **Joseph J. Berry**: Conceptualization, Supervision, Resources **Matthew S. White** Conceptualization, Writing - review & editing, Supervision, Project administration.

Declaration of Competing Interest

The authors have no competing interests.

Acknowledgements

This material is based upon work supported by the National Science Foundation under Grant No. OIA-1738575. This work was authored by the National Renewable Energy Laboratory, operated by Alliance for Sustainable Energy, LLC, for the U.S. Department of Energy (DOE) under Contract No. DE-AC36-08GO28308. This material is based upon work supported by the U.S. Department of Energy?s Office of Energy Efficiency and Renewable Energy (EERE) under the Solar Energy Technologies Office (SETO) project “De-risking Halide Perovskite Solar Cells” program (DE-FOA-0000990). The views expressed in the article do not necessarily represent the views of the DOE or the U.S. Government. The U.S. Government retains and the publisher, by ac- cepting the article for publication, ac-

knowledges that the U.S. Government retains a nonexclusive, paid-up, irrevocable, worldwide license to publish or reproduce the published form of this work, or allow others to do so, for U.S. Government purposes. B.D., B.I., and O.S. thank the financial support from the UVM Office of Fellowships, Opportunities, and Undergraduate Research (FOUR) Clean Energy Fund.

References

[1] S. Rühle, A. Y. Anderson, H.-N. Barad, B. Kupfer, Y. Bouhadana, E. Rosh-Hodesh, A. Zaban, All-Oxide Photovoltaics, The Journal of Physical Chemistry Letters 3 (24) (2012) 3755–3764.

[2] M. S. Dabney, M. F. van Hest, C. W. Teplin, S. P. Arenkiel, J. D. Perkins, D. S. Ginley, Pulsed laser deposited Nb doped TiO_2 as a transparent conducting oxide, Thin Solid Films 516 (12) (2008) 4133–4138.

[3] M. Taylor, D. Readey, C. Teplin, M. F. van Hest, J. Alleman, M. Dabney, L. Gedvilas, B. Keyes, B. To, J. Perkins, The electrical, optical and structural properties of $In_xZn_{1-x}O_y$ ($0 \leq x \leq 1$) thin films by combinatorial techniques, Measurement Science & Technology 16 (2005) 90–94.

[4] E. Fortunato, D. S. Ginley, H. Hosono, D. C. Paine, Transparent conducting oxides for photovoltaics, Mrs Bulletin 32 (3) (2007) 242–247.

[5] M. S. White, D. C. Olson, S. E. Shaheen, N. Kopidakis, D. S. Ginley, Inverted bulk-heterojunction organic photovoltaic device using a solution-derived ZnO underlayer, Applied Physics Letters 89 (14) (2006) 143517.

[6] C. Platzer-Björkman, T. Törndahl, D. Abou-Ras, J. Malmström, J. Kessler, L. Stolt, Zn(O,S) buffer layers by atomic layer deposition in $Cu(In,Ga)Se_2$ based thin film solar cells: Band alignment and sulfur gradient, Journal of Applied Physics 100 (4) (2006) 044506–10.

[7] M. T. Htay, Y. Hashimoto, N. Momose, K. Sasaki, H. Ishiguchi, S. Igarashi, K. Sakurai, K. Ito, A Cadmium-Free Cu_2ZnSnS_4/ZnO Hetrojunction Solar Cell Prepared by Practicable Processes, Japanese Journal of Applied Physics 50 (2011) 032301–5.

[8] M. Liu, M. B. Johnston, H. J. Snaith, Efficient planar heterojunction perovskite solar cells by vapour deposition, Nature 501 (7467) (2013) 395–398.

[9] M. S. White, D. C. Olson, N. Kopidakis, A. M. Nardes, D. S. Ginley, J. J. Berry, Control of charge separation by electric field manipulation in polymer-oxide hybrid organic photovoltaic bilayer devices, physica status solidi (a) 207 (5) (2010) 1257–1265.

[10] K. X. Steirer, P. F. Ndione, N. E. Widjonarko, M. T. Lloyd, J. Meyer, E. L. Ratcliff, A. Kahn, N. R. Armstrong, C. J. Curtis, D. S. Ginley, J. J. Berry, D. C. Olson, Enhanced Efficiency in Plastic Solar Cells via Energy Matched Solution Processed NiOx Interlayers, Advanced Energy Materials 1 (5) (2011) 813–820.

[11] M. D. Heinemann, M. F. van Hest, M. Contreras, J. D. Perkins, A. Zakutayev, C. A. Kaufmann, T. Unold, D. S. Ginley, J. J. Berry, Amorphous oxides as electron transport layers in $Cu(In,Ga)Se_2$ superstrate devices, physica status solidi (a) 214 (5) (2017) 1600870–6.

[12] P. F. Ndione, A. Garcia, N. E. Widjonarko, A. K. Sigdel, K. X. Steirer, D. C. Olson, P. A. Parilla, D. S. Ginley, N. R. Armstong, R. E. Richards, E. L. Ratcliff, J. J. Berry, Highly-Tunable Nickel Cobalt Oxide as a Low-Temperature P-Type Contact in Organic Photovoltaic Devices, Advanced Energy Materials 3 (4) (2012) 524–531.

[13] M. M. Lee, J. Teuscher, T. Miyasaka, T. N. Murakami, H. J. Snaith, Efficient Hybrid Solar Cells Based on Meso-Superstructured Organometal Halide Perovskites, Science 338 (6107) (2012) 643–647.

[14] D. C. Olson, J. Piris, R. T. Collins, S. E. Shaheen, D. S. Ginley, Hybrid photovoltaic devices of polymer and ZnO nanofiber composites, Thin Solid Films 496 (1) (2006) 26–29.

[15] W. Beek, M. M. Wienk, R. A. J. Janssen, Efficient hybrid solar cells from zinc oxide nanoparticles and a conjugated polymer, Advanced Materials 16 (12) (2004) 1009–1013.

[16] T. S. Gershon, A. K. Sigdel, A. T. Marin, M. F. van Hest, D. S. Ginley, R. H. Friend, J. L. MacManus-Driscoll, J. J. Berry, Improved fill factors in solution-processed ZnO/Cu2O photovoltaics, Thin Solid Films 536 (C) (2013) 280–285.

[17] X. Yin, Z. Xu, Y. Guo, P. Xu, M. He, Ternary Oxides in the TiO_2–ZnO System as Efficient Electron-Transport Layers for Perovskite Solar Cells with Efficiency over 15%, ACS Applied Materials & Interfaces 8 (43) (2016) 29580–29587.

[18] W. Ke, G. Fang, Q. Liu, L. Xiong, P. Qin, H. Tao, J. Wang, H. Lei, B. Li, J. Wan, G. Yang, Y. Yan, Low-Temperature Solution-Processed Tin Oxide as an Alternative Electron Transporting Layer for Efficient Perovskite Solar Cells, Journal Of The American Chemical Society 137 (21) (2015) 6730–6733.

[19] J. Song, J. Bian, E. Zheng, X.-F. Wang, W. Tian, T. Miyasaka, Efficient and Environmentally Stable Perovskite Solar Cells Based on ZnO Electron Collection Layer, Chemistry Letters 44 (5) (2015) 610–612.

[20] Z. Li, Stable Perovskite Solar Cells Based on WO_3 Nanocrystals as Hole Transport Layer, Chemistry Letters 44 (8) (2015) 1140–1141.

[21] S. Seo, I. J. Park, M. Kim, S. Lee, C. Bae, H. S. Jung, N.-G. Park, J. Y. Kim, H. Shin, An ultra-thin, un-doped NiO hole transporting layer of highly efficient (16.4%) organic–inorganic hybrid perovskite solar cells, Nanoscale 8 (22) (2016) 11403–11412.

[22] C.-S. Jiang, M. Yang, Y. Zhou, B. To, S. U. Nanayakkara, J. M. Luther, W. Zhou, J. J. Berry, J. Van De Lagemaat, N. P. Padture, K. Zhu, M. M. Al-Jassim, Carrier separation and transport in perovskite solar cells studied by nanometre-scale profiling of electrical potential, Nature Communications 6 (2015) 8397–10.

[23] D. C. Olson, S. E. Shaheen, M. S. White, W. J. Mitchell, M. F. van Hest, R. T. Collins, D. S. Ginley, Band-Offset Engineering for Enhanced Open-Circuit Voltage in Polymer–Oxide Hybrid Solar Cells, Advanced Functional Materials 17 (2) (2007) 264–269.

[24] H. M. Christen, G. Eres, Recent advances in pulsed-laser deposition of complex oxides, Journal Of Physics-Condensed Matter 20 (26) (2008) 264005–17.

[25] L. W. Martin, Y. H. Chu, R. Ramesh, Advances in the growth and characterization of magnetic, ferroelectric, and multiferroic oxide thin films, Materials Science & Engineering R-Reports 68 (4-6) (2010) 89–133.

[26] H. N. Lee, H. M. Christen, M. F. Chisholm, C. M. Rouleau, D. H. Lowndes, Strong polarization enhancement in asymmetric three-component ferroelectric superlattices, Nature 433 (7024) (2005) 395–399.

[27] J. Z. Tischler, G. Eres, B. C. Larson, C. M. Rouleau, P. Zschack, D. H. Lowndes, Nonequilibrium Interlayer Transport in Pulsed Laser Deposition, Physical Review Letters 96 (22) (2006) 226104–4.

[28] W. Geißelbrecht, U. Pfeiffer, A. Thränhardt, U. Klütz, An optimized digital alloy growth technique for accurate band gap engineering, Journal of Crystal Growth (1999).

[29] M. G. Peters, B. J. Thibeault, D. B. Young, J. W. Scott, F. H. Peters, A. C. Gossard, L. A. Coldren, Band-gap engineered digital alloy interfaces for lower resistance vertical-cavity surface-emitting lasers, Applied Physics Letters 63 (25) (1993) 3411–3413.

[30] M. Asif Khan, J. N. Kuznia, D. T. Olson, T. George, W. T. Pike, GaN/AlN digital alloy short-period superlattices by switched atomic layer metalorganic chemical vapor deposition, Applied Physics Letters 63 (25) (1993) 3470–3472.

[31] R. Kaspi, G. P. Donati, Digital alloy growth in mixed As/Sb heterostructures, Journal of Crystal Growth 251 (1-4) (2003) 515–520.

[32] Y. G. Hong, A. Y. Egorov, C. W. Tu, Growth of GaInNAs quaternaries using a digital alloy technique, Journal of Vacuum Science & Technology B: Microelectronics and Nanometer Structures 20 (3) (2002) 1163–5.

[33] D. H. Kim, H. N. Lee, M. D. Biegalski, H. M. Christen, Large ferroelectric polarization in antiferromagnetic $BiFe_{0.5}Cr_{0.5}O_3$ epitaxial films, Applied Physics Letters 91 (4) (2007) 042906–4.

[34] L. Miéville, T. H. Geballe, L. Antognazza, K. Char, Ti and Ca substitution in $SrRuO_3$ thin films by sequential deposition process, Applied Physics Letters 70 (1) (1997) 126–4.

[35] H. M. Christen, L. A. Boatner, J. D. Budai, M. F. Chisholm, L. A. Géa, P. J. Marrero, D. P. Norton, The growth and properties of epitaxial $KNbO_3$ thin films and $KNbO_3/KTaO_3$ superlattices, Applied Physics Letters 68 (11) (1996) 1488–4.

[36] H. Tabata, H. Tanaka, T. Kawai, Formation of artificial $BaTiO_3/SrTiO_3$ superlattices using pulsed laser deposition and their dielectric properties, Applied Physics Letters 65 (15) (1994) 1970–4.

[37] G. Q. Gong, A. Gupta, G. Xiao, P. Lecoeur, T. R. McGuire, Perovskite oxide superlattices: Magnetotransport and magnetic properties, Physical Review B 54 (6) (1996) R3742–R3745.

[38] C. Kwon, Q. Li, K. C. Kim, M. C. Robson, Z. Trajanovic, J. L. Peng, R. L. Greene, A. M. Repaci, C. Lobb, R. Decca, H. D. Drew, R. Ramesh,

T. Venkatesan, K. M. Ham, R. Sooryakumar, Pulsed laser deposited superlattices based on perovskite oxides, Superlattices And Microstructures 19 (3) (1996) 169–181.
[39] P. A. Salvador, A. M. Haghiri-Gosnet, B. Mercey, M. Hervieu, B. Raveau, Growth and magnetoresistive properties of $(LaMnO_3)_m(SrMnO_3)_n$ superlattices, Applied Physics Letters 75 (17) (1999) 2638–4.
[40] P. R. Willmott, S. A. Pauli, R. Herger, C. M. Schlepütz, D. Martoccia, B. D. Patterson, B. Delley, R. Clarke, D. Kumah, C. Cionca, Y. Yacoby, Structural Basis for the Conducting Interface between $LaAlO_3$ and $SrTiO_3$, Physical Review Letters 99 (15) (2007) 155502–4.
[41] K. Ueda, H. Tabata, T. Kawai, Ferromagnetism in $LaFeO_3$-$LaCrO_3$ Superlattices, Science 280 (5366) (1998) 1064–1066.
[42] H. M. Christen, S. D. Silliman, K. Harshavardhan, Epitaxial superlattices grown by a PLD-based continuous compositional-spread technique, Applied Surface Science 189 (2002) 216–221.
[43] T. Choi, B. H. Park, H. Shin, J. Lee, Nano-domain engineering in ultrashort-period ferroelectric superlattices, Applied Physics Letters 100 (22) (2012) 222906–5.
[44] A. Ohtomo, M. Kawasaki, Y. Sakurai, I. Ohkubo, Fabrication of alloys and superlattices based on ZnO towards ultraviolet laser, Materials Science and Engineering B 56 (2-3) (1998) 263–266.
[45] A. Ohtomo, M. Kawasaki, T. Koida, K. Masubuchi, H. Koinuma, Y. Sakurai, Y. Yoshida, T. Yasuda, Y. Segawa, $Mg_xZn_{1-x}O$ as a II-VI widegap semiconductor alloy, Applied Physics Letters 72 (19) (1998) 2466–2468.
[46] A. Ohtomo, A. Tsukazaki, Pulsed laser deposition of thin films and superlattices based on ZnO, Semiconductor Science and Technology 20 (4) (2005) S1–S12.
[47] A. Ohtomo, K. Tamura, M. Kawasaki, T. Makino, Y. Segawa, Z. K. Tang, G. K. L. Wong, Y. Matsumoto, H. Koinuma, Room-temperature stimulated emission of excitons in ZnO/(Mg,Zn)O superlattices, Applied Physics Letters 77 (14) (2000) 2204–4.
[48] A. Ohtomo, M. Kawasaki, I. Ohkubo, H. Koinuma, T. Yasuda, Y. Segawa, Structure and optical properties of ZnO/$Mg_{0.2}Zn_{0.8}O$ superlattices, Applied Physics Letters 75 (7) (1999) 980–4.
[49] Y. Ke, J. J. Berry, P. Parilla, A. Zakutayev, R. O'Hayre, D. S. Ginley, The origin of electrical property deterioration with increasing Mg concentration in ZnMgO:Ga, Thin Solid Films 520 (9) (2012) 3697–3702.
[50] K. Ellmer, Magnetron sputtering of transparent conductive zinc oxide: relation between the sputtering parameters and the electronic properties, Journal Of Physics D-Applied Physics 33 (2000) R17–R32.
[51] K. Ellmer, Resistivity of polycrystalline zinc oxide films: current status and physical limit, Journal Of Physics D-Applied Physics 34 (21) (2001) 3097–3108.
[52] T. Yamamoto, Dependence of carrier concentrations on oxygen pressure for Ga-doped ZnO prepared by ion plating method, Thin Solid Films 451-452 (2004) 439–442.
[53] S. Tanaka, A. A. Zakhidov, R. Ovalle-Robles, Y. Yoshida, I. Hiromitsu, Y. Fujita, K. Yoshino, Semitransparent organic photovoltaic cell with carbon nanotube-sheet anodes and Ga-doped ZnO cathodes, Synthetic Metals 159 (21-22) (2009) 2326–2328.
[54] C. Harada, H. Ko, H. Makino, T. Yao, Phase separation in Ga-doped MgZnO layers grown by plasma-assisted molecular-beam epitaxy, Materials Science in Semiconductor Processing 6 (5-6) (2003) 539–541.
[55] B. Dou, L. M. Wheeler, J. A. Christians, D. T. Moore, S. P. Harvey, J. J. Berry, F. S. Barnes, S. E. Shaheen, M. F. van Hest, Degradation of Highly Alloyed Metal Halide Perovskite Precursor Inks: Mechanism and Storage Solutions, ACS Energy Letters 3 (4) (2018) 979–985.
[56] G. Rao, F. Sauberlich, A. Klein, Influence of Mg content on the band alignment at CdS/(Zn,Mg)O interfaces, Applied Physics Letters 87 (3) (2005) 032101.
[57] Y. Ke, S. Lany, J. J. Berry, J. D. Perkins, P. A. Parilla, A. Zakutayev, T. Ohno, R. O'Hayre, D. S. Ginley, Enhanced Electron Mobility Due to Dopant-Defect Pairing in Conductive ZnMgO, Advanced Functional Materials 24 (19) (2014) 2875–2882.
[58] J. A. Christians, P. Schulz, J. S. Tinkham, T. H. Schloemer, S. P. Harvey, B. J. T. de Villers, A. Sellinger, J. J. Berry, J. M. Luther, Tailored interfaces of unencapsulated perovskite solar cells for >1,000 hour operational stability, Nature Energy 3 (1) (2018) 1–7.
[59] M. Quintana, T. Edvinsson, A. Hagfeldt, G. Boschloo, Comparison of Dye-Sensitized ZnO and TiO_2Solar Cells: Studies of Charge Transport and Carrier Lifetime, The Journal of Physical Chemistry C 111 (2) (2007) 1035–1041.
[60] H. Minoura, T. Yoshida, Electrodeposition of ZnO/dye hybrid thin films for dye-sensitized solar cells, Electrochemistry 76 (2) (2008) 109–117.
[61] T. Feurer, P. Reinhard, E. Avancini, B. Bissig, J. Löckinger, P. Fuchs, R. Carron, T. P. Weiss, J. Perrenoud, S. Stutterheim, S. Buecheler, A. N. Tiwari, Progress in thin film CIGS photovoltaics - Research and development, manufacturing, and applications, Progress in Photovoltaics: Research and Applications 25 (7) (2016) 645–667.
[62] J. Yang, B. D. Siempelkamp, E. Mosconi, F. De Angelis, T. L. Kelly, Origin of the Thermal Instability in $CH_3NH_3PbI_3$Thin Films Deposited on ZnO, Chemistry Of Materials 27 (12) (2015) 4229–4236.
[63] R. C. Shallcross, S. Olthof, K. Meerholz, N. R. Armstrong, Understanding the role of titanium dioxide (TiO2) surface chemistry on the nucleation and energetics of hybrid perovskite films (Conference Presentation), in: K. Lee, Z. H. Kafafi, P. A. Lane (Eds.), Organic, Hybrid, and Perovskite Photovoltaics XVIII, SPIE, 2017, p. 48.
[64] E. M. Miller, Y. Zhao, C. C. Mercado, S. K. Saha, J. M. Luther, K. Zhu, V. Stevanović, C. L. Perkins, J. Van De Lagemaat, Substrate-controlled band positions in $CH_3NH_3PbI_3$perovskite films, Physical Chemistry Chemical Physics 16 (40) (2014) 22122–22130.
[65] C. Bi, B. Chen, H. Wei, S. DeLuca, J. Huang, Efficient Flexible Solar Cell based on Composition-Tailored Hybrid Perovskite, Advanced Materials 29 (30) (2017) 1605900–6.
[66] B. Dou, E. M. Miller, J. A. Christians, E. M. Sanehira, T. R. Klein, F. S. Barnes, S. E. Shaheen, S. M. Garner, S. Ghosh, A. Mallick, D. Basak, M. F. van Hest, High-Performance Flexible Perovskite Solar Cells on Ultrathin Glass: Implications of the TCO, The Journal of Physical Chemistry Letters 8 (19) (2017) 4960–4966.